Journal of Polymers and the Environment (2022) 30:4287–4303
https://doi.org/10.1007/s10924-022-02508-z

ORIGINAL PAPER

Preparation of Lignin Sulfonate Based/Organo-Montmorillonite Composite Hydrogel for Adsorbing Methylene Blue from Aqueous Solution

Liang Shi[1] · **Wenwu Liu**[1] · **Xiaomei Zhang**[1] · **Jingsong Hu**[1]

Accepted: 6 June 2022 / Published online: 4 July 2022

Abstract

In this study, an environmentally friendly lignin-based hybrid hydrogel (LS/OMMT) was prepared by grafting of acrylamide (AM) and acrylic acid (AA) onto calcium lignosulfonate (LS) and homogeneously distributing organic montmorillonite (OMMT) using an ultrasonic technique. FT-IR, XRD, TGA, SEM, EDS, BET, and XPS were used to characterize the physicochemical and structural properties of LS/OMMT. Then, LS/OMMT was applied to remove methylene blue (MB) from an aqueous solution and a systematic study of pH, contact time and initial MB concentration was carried out. The MB adsorption capacity on LS/OMMT was up to 492.7 mg g^{-1} at 313.15 K and pH 7.0. The Langmuir model well described the MB adsorption on LS/OMMT and the calculated thermodynamic parameters, such as ΔG°, ΔH°, and ΔS°, suggested that MB adsorption on LS/OMMT was spontaneous and endothermic. LS/OMMT adsorption of MB followed a pseudo-second-order kinetic model. Electrostatic attraction and hydrogen-bonding interaction were the mechanisms of adsorption. As a result, this study illustrates that LS/OMMT is an environmentally friendly and efficient adsorbent for wastewater treatment applications.

Keywords Lignin based hydrogel · Organo-montmorillonite · Adsorption · Methylene blue

Introduction

Cationic dyes are extensively used in various industries, including papermaking, textile coloration, coatings, cosmetics, and food processing [1]. When untreated dye effluent is dumped directly into water, it can impact the ecosystem and human health via the food chain. Methylene blue (MB) is a cationic dye that can be carcinogenic and mutagenic during degradation [2]. Moreover, it can induce unpleasant symptoms, including retching, shock, jaundice, cyanosis, tissue necrosis, and even neurological harm [3]. As a result, it is critical and urgent to develop effective methods for the removal of MB from industrial effluents [4]. Therefore, many researchers are interested in removing dyes from aqueous solutions. Adsorption [5], photodegradation [6], flocculation [7], oxidation–reduction [8], and membrane filtration [9] have been employed. Adsorption has become one of the research hotspots among these methods due to its advantages of simple operation, low cost, and recyclability [10]. Therefore, it is challenging to design an adsorbent with excellent selectivity, efficiency, and stability for dye-containing wastewater. So far, adsorbents based on clay [11], activated carbon [12], zeolite [13], metal–organic framework (MOF) [14], and other materials have been reported [15].

Biopolymer hydrogel are three-dimensional network polymer materials made from renewable feedstocks such as starch [16], cellulose [17], chitin/chitosan [18], lignin [19], and agricultural wastes [20]. As the functional groups of biopolymer hydrogel can interact with metal ions or dye molecules, they have shown significant prospects as absorbents for cationic dyes. In addition, these absorbents offer additional advantages over conventional ones, such as low cost, biodegradability, high usability, and high adsorption efficiency [21].

Lignosulfonate (LS), a result of acid pulping, is abundant in the black effluent of pulp mills, has good biocompatibility and is environmental friendliness [22]. Due to its aromatic properties and functional groups (alcoholic and phenolic hydroxyl groups), LS is an attractive candidate for high-performance

---

✉ Liang Shi
446895451@qq.com

[1] College of Chemical Engineering, Anhui University of Science and Technology, Huainan 232001, Anhui, People's Republic of China

adsorbents among the biopolymer classes [23]. Chemical treatments, such as cross-linking and graft copolymerization, are required to make LS insoluble in water and boost their adsorption properties and improve their use for adsorbing cationic dyes and metal ions. For example, Yu et al. prepared a lignin-based hydrogel (LS-g-AA) by grafting acrylic acid (AA) on the backbone of LS in the presence of N, N'-methylene bis (acrylamide) (MBA) [24]. Shi et al. prepared a lignin-based composite (lignin-PEI) by cross-linking the lignin matrix with polyethyleneimine, which was then used to adsorb Ni^{2+} in polluted water [25].

Compared to biopolymer hydrogel, biopolymer/inorganic composite hydrogel exhibits outstanding thermal and mechanical properties [26]. Montmorillonite (MMT) is a layered aluminum silicate composed of octahedral aluminum and tetrahedral silica sheets [27]. It is commonly employed as an adsorbent to remove dyes and heavy metals [28]. The layer structure characteristics and the weak interaction forces between layers make MMT easily organised by the surfactants through an ion-exchange process, which ultimately results in organic montmorillonite (OMMT). As OMMT has a more pronounced layer spacing than MMT, it is easier to exfoliate as a nano-sheet during polymerization. Biopolymer/OMMT composites are highly effective in the removal of heavy metals, dyes, and pesticides from water [19, 29]. Currently, there are only a few reports exist on biopolymer/OMMT composite as an absorbent for wastewater remediation. For example, calcium alginate/OMMT composites can be potent in the rapid removal of anionic dyes from water due to their greater specific surface area and porosity [30]. Wu et al. reported a study on the synthesis of cellulose-g-poly(methyl methacrylate)/OMMT and its application in the removal of 2,4-dichlorophenol (2,4-DCP) from aqueous solution [31].

As mentioned above, LS, a natural biopolymer and OMMT, a clay mineral with a higher specific surface area and reactive –OH groups, are promising candidates for creating a cost-effective and environmentally friendly composite adsorbent. As a result, a new OMMT-containing hybrid hydrogel (LS/OMMT) was prepared, which was made by grafting acrylamide(AM) and acrylic acid (AA) onto LS. Then, LS/OMMT composite hydrogel was used to remove MB from wastewater. A study was conducted to investigate the effects of experimental factors (pH, contact time, initial MB concentration, and adsorbent dosage), adsorption kinetics, isotherms, and thermodynamics on the adsorption performance of LS/OMMT for MB and the adsorption mechanism was also postulated.

Experiment

Materials

AA, AM, MB, MBA, NaOH, and potassium persulfate (KPS) were all of analytical grade and purchased from Aladdin Reagent of China. Hydrochloric acid (HCl, 37 wt%) was purchased from Sinopharm Chemical Reagent Co., LS. OMMT was of chemically grade and purchased from Tianjin Kermel Chemical Reagent Co., Ltd. All other chemicals were purchased and used unless otherwise specified. Deionized water of high purity was utilized in the study.

Instruments

Fourier transform infrared spectroscopy (FT-IR) was recorded using a Nicolet is50 spectrophotometer in 400–4000 cm^{-1}. X-ray diffraction (XRD) patterns were obtained using a Smartlab SE X-ray diffractometer with a Cu-K radiation source operating at 40 kV, 30 mA in the scanning range of $2\theta = 2–30°$ and 1° min^{-1} scan rate. The surface morphology and chemical composition of LS/OMMT, LS, and OMMT samples were studied using a FlexSEM1000 scanning electron microscope (SEM) with an energy-dispersive X-ray spectroscopy (EDS) detector (IXRF Model 550i). Nestal TG209F1 instrument was used to perform thermal gravimetric analysis (TGA) in N_2 from 20 to 900 °C at a heating rate of 10 °C min^{-1}. Thermo Electron's VG ESCALAB 250Xi spectrometer was applied for X-ray photoelectron spectroscopy (XPS) with an Al K X-ray source (1486 eV). LS/OMMT porosity was studied by using the N_2 adsorption/desorption isotherm at 77 K, which included BET (SA3100) specific surface area, pore size, and pore volume.

Preparation of LS/OMMT Composite Hydrogel

LS/OMMT composite hydrogel was prepared according to a similar procedure described previously [19]. Graft copolymerization of AA and AM onto LS in the presence of chemical cross-linker MBA, initiator KPS, and OMMT produced the LS/OMMT hydrogel. The standard procedure was as follows: LS (1.5 g), AA (6.0 g, partially neutralized by 10 mL of 6 mol L^{-1} sodium hydroxide solution), AM (3.0 g), and OMMT(1.2 g) were added to a 250 mL beaker and ultrasonically dispersed for 1 h at room temperature. The mixture was added to a four-neck flask with a mechanical stirrer, a reflux condenser, and a nitrogen line. After the addition of the initiator KPS (0.25 g) and the crosslinker MBA (0.75 g), the temperature was gradually increased to 70 °C and held for 2 h. The obtained products were soaked in deionized water for two days and the deionized water was changed periodically to remove homopolymers and unreacted monomers [32]. Finally, the composite hydrogel was dried at 60 °C, and the dried samples were ground for further testing. This method of preparing LS/OMMT composite hydrogel and the mechanism of formation is shown schematically in Fig. 1.

Adsorption Experiments

The effects of pH, adsorbent dosage, and initial MB concentration on dye adsorption were explored using batch adsorption experiments. In conclusion, a specific amount of LS/OMMT was added to 150 mL flasks and contacted 100 mL of the desired concentration of dye solution. The adsorbent was separated by filtration after shaking the mixture at 150 rpm at a regulated temperature. The change in absorbance of the maximum absorbance (665 nm) was monitored using a UV–vis spectrophotometer to determine the concentrations of the MB solution before and after adsorption. The adsorption capacity at equilibrium (Q_e, mg g^{-1}) as well as at time t (Q_t, mg g^{-1}) and removal ratio (RR) were calculated by the following equations:

$$Q_e = \frac{C_0 - C_e}{m}V \tag{1}$$

$$Q_t = \frac{C_0 - C_t}{m}V \tag{2}$$

$$RR = \frac{C_0 - C_e}{C_0} \times 100\% \tag{3}$$

where C_0 (mg L^{-1}), C_t (mg L^{-1}), and C_e (mg L^{-1}) are the concentration of MB at time 0, time t and equilibrium, respectively; m (g) is the amount of the adsorbent and V (L) is the volume of MB solution.

The effect of pH was studied within the range of 1.0 to 10.0 (adjusted with 0.1 mol L^{-1} HCl or NaOH) with a contact time of 140 min at 293.15 K and the C_0 of 50 mg L^{-1}. Adsorption isotherms were conducted at various C_0 (50–600 mg L^{-1}) and various temperatures (283.15 K, 293.15 K, 303.15 K, 313.15 K). Adsorption kinetics studies were performed with 0.1 g LS/OMMT in 200 mL of four different initial dye concentrations, i.e., 100 mg L^{-1},

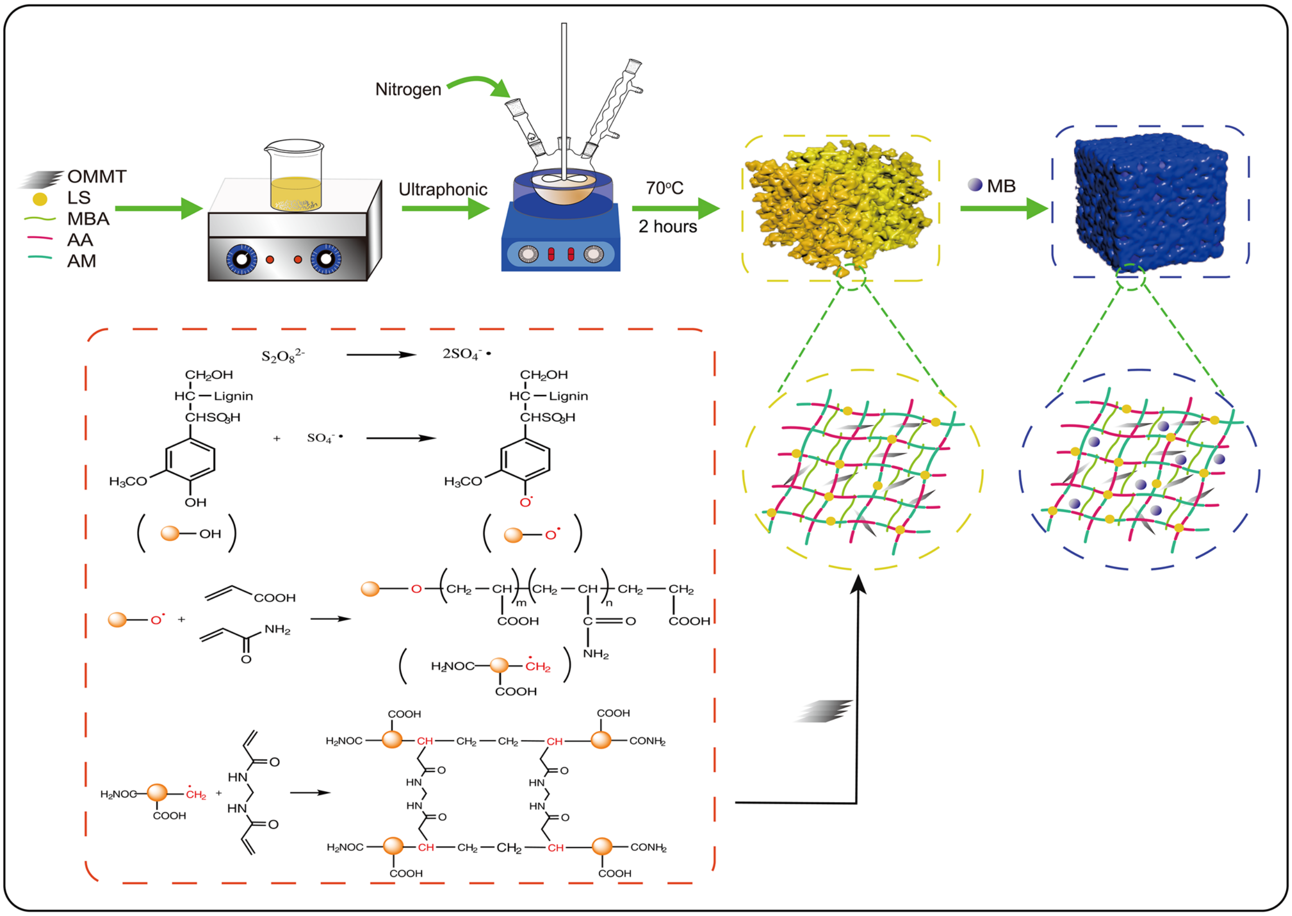

Fig. 1 The preparation method and mechanism for forming the LS/OMMT composite hydrogel

200 mg L^{-1}, 300 mg L^{-1},400 mg L^{-1} at pH 7.0 under 150 rpm. Samples were collected and centrifuged at 4000 rpm for 2 min at predetermined time intervals. Q_t was calculated from Eq. (2).

The point of zero charges (pH_{pzc}) of LS/OMMT were determined using the solid addition method [33]. The experiment was carried out in a series of 100 mL flares containing 50 mL 0.01 mol L^{-1} KCl. The pH was adjusted over a range of 1–11 using HCl (0.01 mol L^{-1}) or NaOH (0.01 mol L^{-1}). The pH of initial solutions was measured and noted as pH_0. After a constant value of pH_0 was reached, 0.15 g of the LS/OMMT was added to each flask. The suspensions were sealed and shaken at 150 rpm and 25 °C for 24 h, and the second pH noted as pH_f was measured. A plot of ΔpH ($\Delta pH = pH_0$—pH_f) vs. pH_0 was made, and pH_{PZC} was the point where the curve cuts the x-axis implying the point when $pH_0 = pH_f$.

Desorption Study and Reusability of Hydrogel

In order to recycle LS/OMMT, the method reported in the literature was adapted with few modifications [31]. LS/OMMT composite hydrogels with adsorbed MB (MB-LS/OMMT) was collected and transferred into deionized water for 1 h to remove un-desorbed MB and then dried in an oven 60 °C for 12 h for desorption experiments. The dried MB-LS/OMMT was then immersed in a solution of HCl (0.1 mol L^{-1}) for 24 h while shaking at 300 rpm. Samples were obtained from the solution to track the amount of MB desorbed and then were treated with NaOH (0.1 mol L^{-1}) solution to regenerate their binding sites after desorbing with HCl solution. Finally, the adsorbents were separated, washed with deionized water, and reused in the next cycle of the adsorption experiment. A total of five cycles of adsorption–desorption experiments were carried out. The amount of MB absorbed onto the LS/OMMT was determined and calculated by RR mentioned above.

Results and Discussion

Characterization

The LS/OMMT FT-IR spectra (Fig. 2) show that the absorption band at 3482 cm^{-1} is attributable to O–H and N–H stretching vibrations and the band at 2941 cm^{-1} is related to C–H stretching vibrations of $-CH_2$ and $-CH_3$ [34]. Aromatic skeleton vibration was responsible for the absorption peak at 1557 cm^{-1} and 1457 cm^{-1}. The peak at 1217 cm^{-1} was assigned to the syringyl structure characteristic absorption peak from lignin [35, 36]. The sulfonic group's typical absorption peaks were 1044 cm^{-1} and 628 cm^{-1} [37]. Two new characteristic signals appear at at 1728 cm^{-1} and 1670 cm^{-1}, respectively, which are attributable to the C=O stretching vibration of carboxylic acid and amide produced from AA and AM [38] compared to the FT-IR spectrum of LS. Also, the C–O (1160 cm^{-1}) [39] stretching vibration peaks were stronger than that of LS, while the C–N stretching vibration and COO– symmetric stretching vibration exhibited absorption peaks at 1182 cm^{-1} and 1405 cm^{-1} [3, 40]. These results showed that the LS is effectively grafted with AA and AM. A peak at 1114 cm^{-1} for the antisymmetric stretching vibration of Si–O–Si overlaps with the asymmetric stretching vibration peak of the sulfonic group (1038 cm^{-1}), which is more acute and shifts to a higher wavenumber than the comparable peak for OMMT. From the FT-IR spectra of LS/OMMT, the peak disappears at at 910 cm^{-1} (Al–OH bending vibration), suggesting that graft copolymerization happens on the surface and within OMMT. In addition, Si–O–Si symmetric stretching vibration and the Si–O–Al stretching vibration possess wavelengths of 800 cm^{-1} and 769 cm^{-1}, respectively. Besides, Si–O–Al bending vibration absorption peak and Si–O–Si bending vibration are at 515 cm^{-1} and 466 cm^{-1} [3, 41], respectively. These results indicate that OMMT enters into the 3D network structure of the hydrogel.

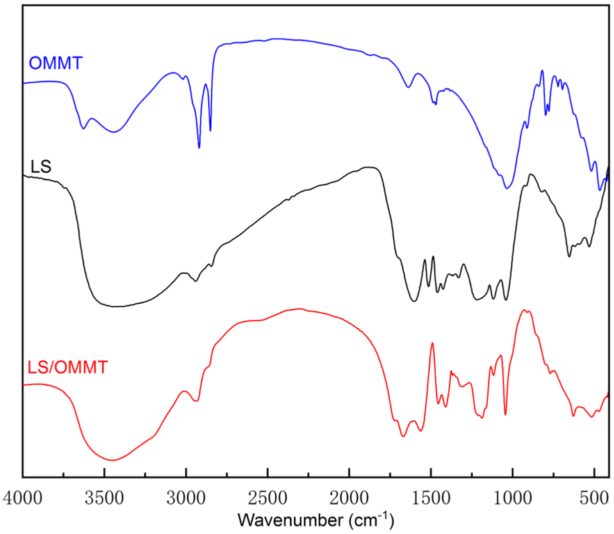

Fig. 2 The FT-IR spectra of LS/OMMT, LS, and OMMT

The XRD patterns for LS/OMMT, LS, and OMMT are shown in Fig. 3. According to relevant literature sources [42, 43], the typical 001 basal reflection peak of MMT is at 2θ = 7.5°°with a d- alue of 11.77 Å. In OMMT, however, this peak was displaced to a lower angle at 2θ = 4.6° with a d value of 19.19 Å. This increase in d value supports the intercalation of surfactants. However, the 001 basal diffraction peak was not present in LS/OMMT, indicating that the LS or the polymer chains entered the OMMT layers during

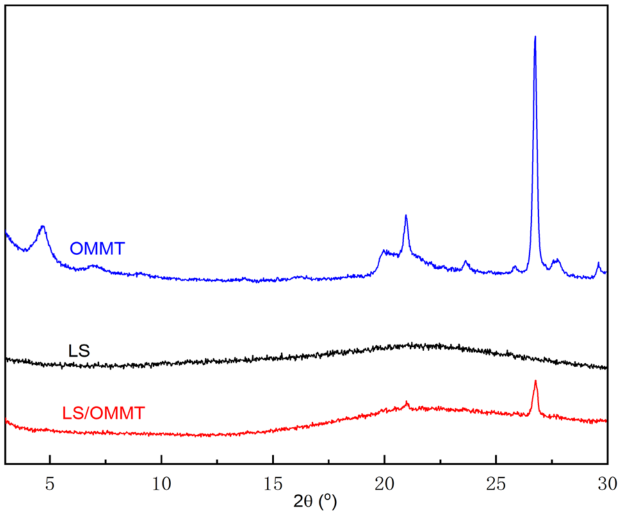

Fig. 3 XRD patterns of LS/OMMT, LS, and OMMT

aqueous solution polymerization, destroying and exfoliating the original layered structure of OMMT [32].

The TGA and DTG curves of LS/OMMT, LS, and OMMT, respectively, are shown in Fig. 4a and b. Four stages of deterioration of LS/OMMT can be observed in the two figures. The first stage, which occurred between 100 and 150 °C and resulted in a 7.5% weight loss, was caused by the physically adsorbed water for LS/OMMT [41]. This is equally responsible for the weight loss for LS (30–125 °C) and OMMT (30–161 °C). In the second stage, between 215 and 300 °C, the weight loss of the sample was about 5%, possibly because the small molecules of LS structure in LS/OMMT began to decompose [25]. Similarly, the tiny molecules of LS were thermally decomposed from 160 to 337 °C, resulting in a 35.6% weight loss. The predominant weight loss of LS/OMMT occurred in the third stage, from 302 to 510 °C, with a weight reduction of 38.6%. Structural degradation of LS and decomposition of acrylic acid and acrylamide polymers from LS/OMMT led to the third stage [4, 44]. In the fourth stage, LS/OMMT lost roughly 4.5% due to OH group breakdown in the OMMT structure at temperatures ranging from 650 to 735 °C [3]. Furthermore, the maximum decomposition temperature of L/SOMMT was 374 °C, which was higher than that of LS (272 °C). These findings suggest that adding OMMT to the polymerization process can improve the thermal stability of the hydrogel.

SEM and EDS analysis were used to study the surface morphology and chemical content of LS/OMMT, LS, and OMMT. Figure 5a–c shows the obtained SEM pictures, while Fig. 6a–c shows the EDS spectrum. Figure 5c showed that the OMMT appears to have a heterogeneous phase and layer structure. The EDS analysis reveals that organic surfactant had been incorporated into the layered structure of MMT, with the presence of C (25.8 wt%) and N (2.19 wt%) in Fig. 6c. The surface of LS/OMMT is significantly rougher compared to LS (Fig. 5b), with many irregular folds in Fig. 5a. LS/OMMT, on the other hand, revealed an uneven macro-porous structure with thinner pore walls. The EDS spectrum of LS/OMMT (Fig. 6a) shows that the LS/OMMT contains the elements Si (2.54 wt%), Al (0.82 wt%), and Fe (0.12 wt%), which further indicates that OMMT successfully enters into the hydrogel matrix. Similar results were reported by Wang et al. [3] and Karaca et al. [45].

The specific surface area and pore size distributions were measured by the N_2 adsorption–desorption experiment at 77 K, and the results are shown in Fig. 7. The pore-size distribution curves of the LS/OMMT, LS, and OMMT are

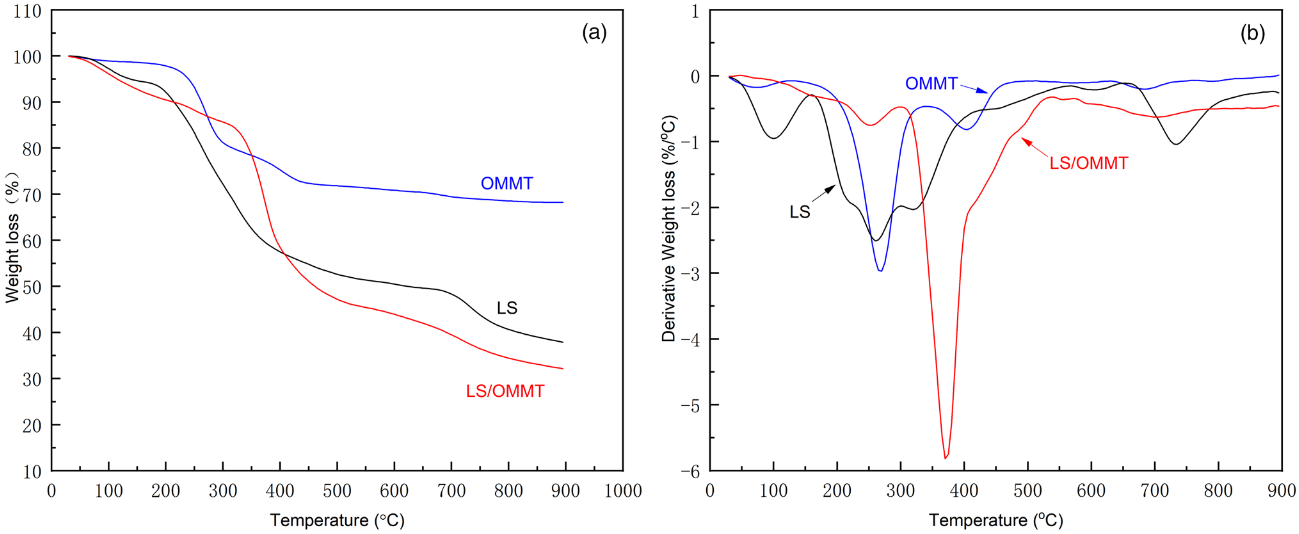

Fig. 4 The TGA curves of LS/OMMT, LS, and OMMT (**a**); the DTG curves of LS/OMMT, LS, and OMMT (**b**)

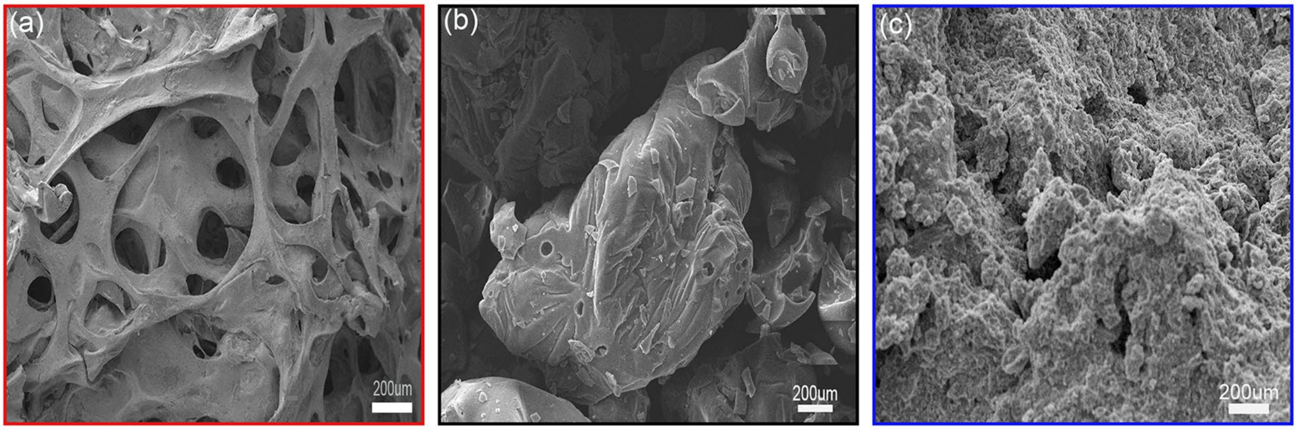

Fig. 5 The SEM of LS/OMMT (**a**), LS (**b**), and OMMT (**c**) at ×500 magnification

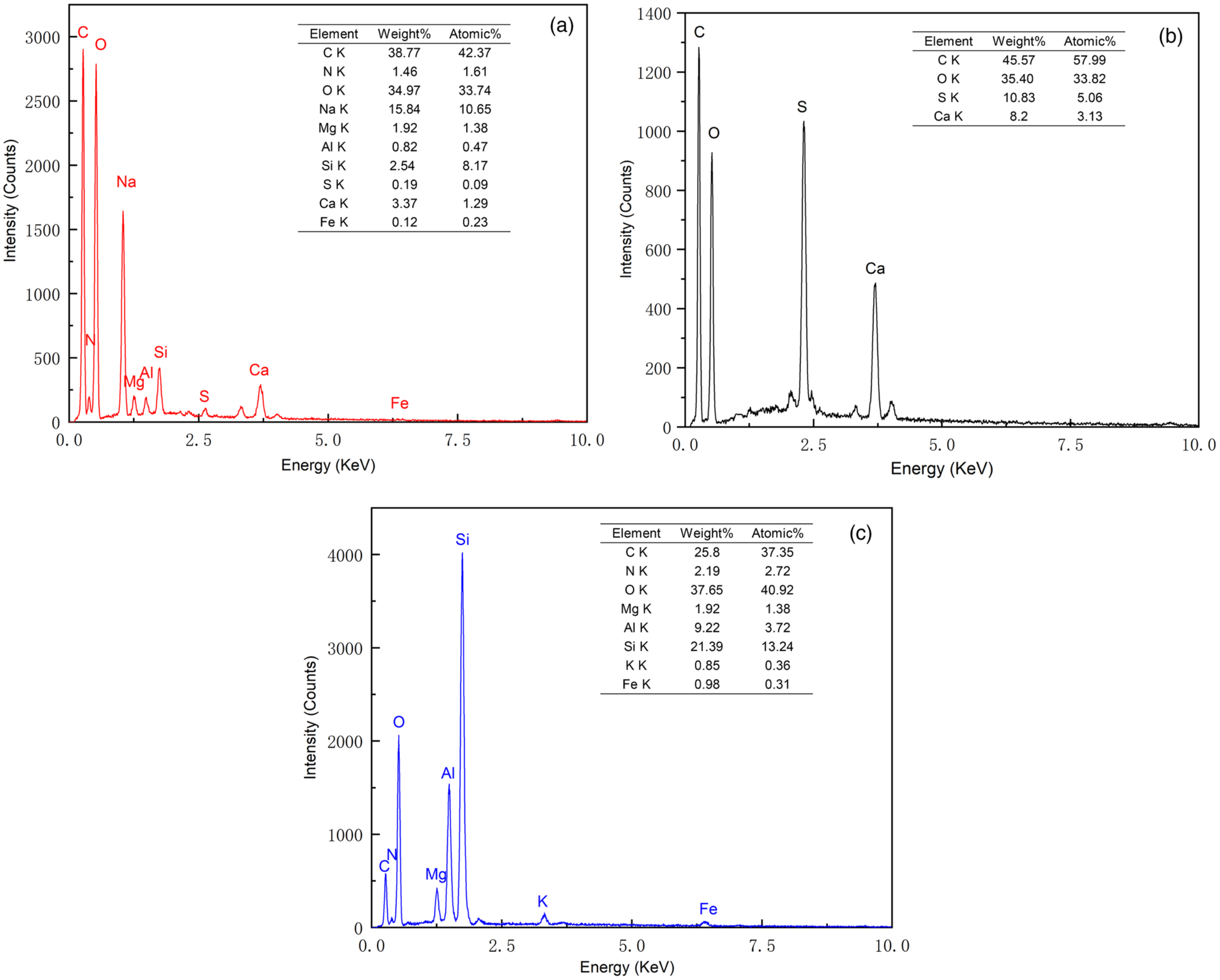

(a)

Element	Weight%	Atomic%
C K	38.77	42.37
N K	1.46	1.61
O K	34.97	33.74
Na K	15.84	10.65
Mg K	1.92	1.38
Al K	0.82	0.47
Si K	2.54	8.17
S K	0.19	0.09
Ca K	3.37	1.29
Fe K	0.12	0.23

(b)

Element	Weight%	Atomic%
C K	45.57	57.99
O K	35.40	33.82
S K	10.83	5.06
Ca K	8.2	3.13

(c)

Element	Weight%	Atomic%
C K	25.8	37.35
N K	2.19	2.72
O K	37.65	40.92
Mg K	1.92	1.38
Al K	9.22	3.72
Si K	21.39	13.24
K K	0.85	0.36
Fe K	0.98	0.31

Fig. 6 The EDS spectrums of LS/OMMT (**a**), LS (**b**), and OMMT (**c**)

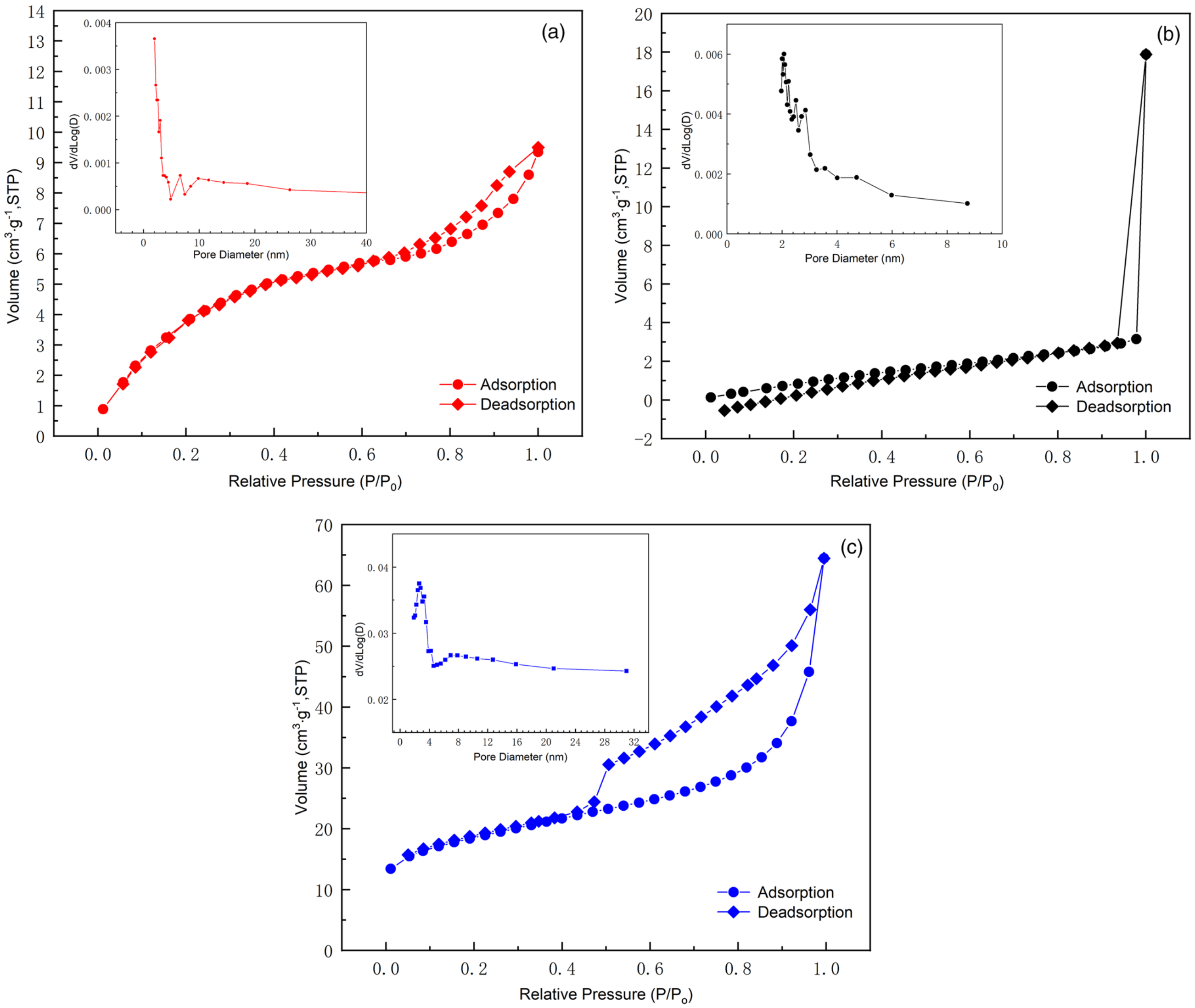

Fig. 7 N_2 adsorption–desorption curves and pore-size distributions for the LS/OMMT (**a**), LS (**b**), and OMMT (**c**)

shown in the insert image. According to Fig. 7c, the isotherm of OMMT is type IV [46, 47], with clear hysteresis loops in the P/P_o range of 0.5–1.0 according to the IUPAC classification, which was the main feature of the type H3 isotherm and ascribed to be typical of of layered materials [48]. The BET surface area (S_{BET}) of OMMT is 62.97 $m^2\ g^{-1}$, as displayed in Table 1, while the average pore diameter (D_{ave}) is 6.206 nm. This result indicates that OMMT has a higher surface area compared to natural MMT reported in the literature [3] and exhibits a mesoporous pore structure [49]. According to Fig. 7b, the isotherm of LS should be attributed to the H1 type, which is typical of polymolecular adsorption [50]. High-pressure hysteresis loops are usually associated with spherical porous structures [51]. In addition, according to the image inserted in Fig. 7b, the pore size distribution of LS is mainly around 2 nm.

Table 1 The surface parameters of the LS/OMMT (a), LS (b), and OMMT (c)

Sample	S_{BET} ($m^2\ g^{-1}$)	V_{tot} ($cm^3\ g^{-1}$)	D_{ave} (nm)
LS/OMMT	6.712	3.943×10^{-4}	3.854
LS	3.136	3.278×10^{-4}	1.819
OMMT	62.97	9.769×10^{-2}	6.206

On the other hand, as seen in Fig. 7a, the isotherm of LS/OMMT is classified with type-IV isotherms [52, 53]. The relative pressure at pressures ($P/P_o > 0.5$) displays a type H4 hysteresis loop [54], which suggests that the LS/OMMT possesses a mesoporous structure [55, 56]. According to Fig. 7a, the pore size distribution is concentrated at 3–10 nm, confirming that the LS/OMMT is mesoporous materials [52].

The uneven pore size distribution of LS/OMMT may be due to the random recombination of polymer monomer and the OMMT during synthesis [53].

The specific surface area values and textural properties are presented in Table 1. The S_{BET} and D_{ave} of LS are 3.136 m^2 g^{-1} and 1.819 nm, respectively, while the S_{BET} and D_{ave} of LS/OMMT are 6.712 m^2 g^{-1} and 3.854 nm, respectively. The above results indicate a substantial increase in surface area due to the incorporation of LS into the OMMT compared to LS. Moreover, the total pore volume (V_{tot}) of the LS/OMMT is also higher than that of LS. However, the lower S_{BET} of the LS/OMMT compared to the OMMT supports the compact incorporation of LS into the OMMT, and consequently causes pore-blocking [57].

Effect of Adsorbent Dosage

The adsorbent dosage determines the adsorbent's ability to remove adsorbate. By changing the adsorbent dose from 0.2 to 0.9 g L^{-1}, the effect of LS/OMMT dosage on MB removal was investigated. Figure 8 shows that when the adsorbent dosage was increased from 0.2 to 0.5 g L^{-1}, the RR increased rapidly from 48.4% to 96.7%. Continue to increase the adsorbent dosage from 0.6 to 0.9 g L^{-1}. RR increases slightly to 98.4% and then remains constant. However, the Q_e drops from 121.1 to 54.7 mg g^{-1} when the dosage of adsorbent increased from 0.2 to 0.9 g L^{-1}. The increase of the amount of adsorbent resulted in the increase of adsorption sites for dye adsorption and the the RR increased. On the other hand, the Q_e per unit mass of adsorbent will decrease because the initial dye concentration was constant [58]. As a result, from an economic and efficiency point of view, the optimal adsorbent dosage for further research was determined to be 0.5 g L^{-1}.

Effect of pH

The pH of the adsorption medium is generally considered to be a critical factor in general as it affects the properties of the adsorbent and adsorbate and the adsorption processes [59]. Figure 9 shows how the Q_e of MB changes with pH. (1.0–10.0). The Q_e increased as the pH went from 1.0 to 7.0 and then tended to level off as the pH went further up. The Q_e of LS/OMMT is greatest when the pH was at 7.0. The protonation-deprotonation process of groups can describe this adsorption performance for RR of MB at variable pH [60]. Excess protons caused functional groups (hydroxyl, phenolic hydroxyl, methoxyl, sulfonic acid, amino) on LS/OMMT to be protonated at $pH < pH_{pzc}$ (6.56, as shown in insert image in Fig. 9) [38]. More positive potential of the LS/OMMT surface and the repulsion of the positively-charged MB prevented the adsorption of MB, leading to a decrease in $Q_{e.}$ In addition, more H^+ compete with dye for binding sites, decreasing the number of active groups available and diminishing the Q_e [48, 49]. At a $pH > pH_{pzc}$, the surface potential of the LS/OMMT became negative due to deionization and electrostatic attraction occurred between the LS/OMMT and MB molecules, thereby enhancing the Q_e. Finally, there is no change in Q_e as the adsorption sites are saturated at pH 7–10.

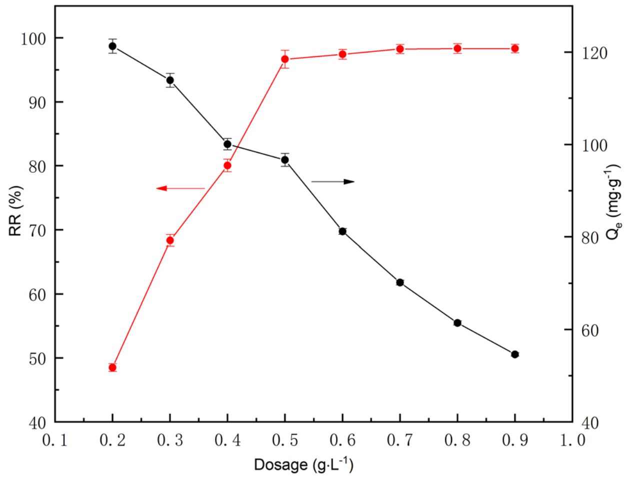

Fig. 8 The effect of LS/OMMT dosage on adsorption of MB (initial MB concentration, 50 mg L^{-1}; pH 7.0; temperature,293.15 K; contact time, 140 min)

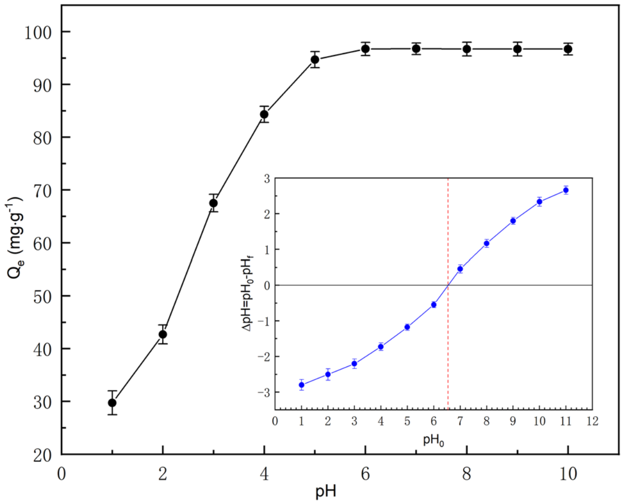

Fig. 9 The effect of pH on adsorption of MB by LS/OMMT (initial MB concentration, 50 mg L^{-1}; absorbent dosage, 0.5 g L^{-1}; temperature, 293.15 K; contact time 140 min)

Effect of Initial Dye Concentration and Adsorption Isotherms

The relationship between the initial MB concentration and the Q_e is crucial for optimizing the adsorption process and comprehending the adsorption behavior. MB solution was introduced into 50 mg of LS/OMMT at four different temperatures (283.15 K, 293.15 K, 303.15 K, and 313.15 K), with C_0 of MB ranging from 50 to 600 mg L^{-1} at pH 7.0. As shown in Fig. 10a, the Q_e improved dramatically when the C_0 increased from 50 to 600 mg L^{-1} because a more significant initial concentration of dye accelerates the adsorption process. Subsequently, as the MB starting concentration was further increased, Q_e slowly increased until it approached equilibrium. This phenomenon is a result of the active sites of the adsorbent being filled and balanced [60]. Furthermore, the Q_e increased with rising temperature. LS/OMMT has a maximum Q_e of 492.7 mg g^{-1} at 313.15 K. This demonstrates that the adsorption of MB on LS/OMMT is an endothermic process.

Adsorption isotherms illustrate how adsorbents interact with the adsorbate and the link between Q_e and C_e. Three adsorption isotherms, including the Langmuir [3], Freundlich [61], and Sips [62] isotherm models, were employed to analyze the experimental data and identify the most suitable isotherm mode.

The Langmuir adsorption isotherm model can be seen as below:

$$Q_e = \frac{Q_{\max} K_L C_e}{1 + K_L C_e} \tag{4}$$

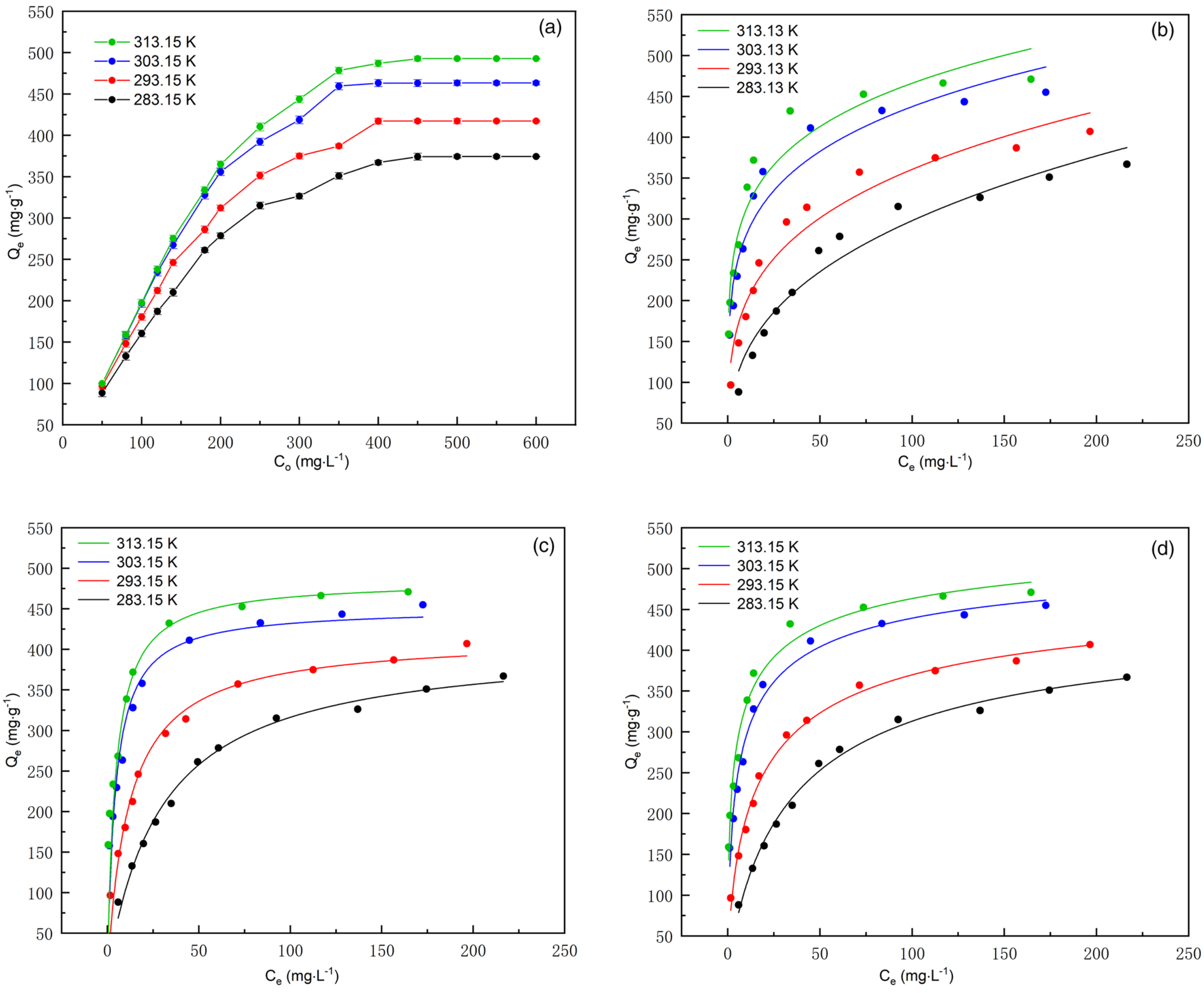

Fig. 10 The effect of initial concentration on adsorption of MB by LS/OMMT (**a**) (pH 7.0; absorbent dosage, 0.5 g L^{-1}; temperature, 283.15 K, 293.15 K, 303.15 K, and 313.15 K; contact time, 140 min)), adsorption isotherms: Langmuir (**b**), Freundlich (**c**) and Sips (**d**)

$$R_L = \frac{1}{1 + K_L C_m} \tag{5}$$

The Freundlich adsorption isotherm model:

$$Q_e = K_F C_e^{1/n} \tag{6}$$

Sips isotherm adsorption isotherm model:

$$Q_e = \frac{Q_S K_S C_e^N}{1 + K_S C_e^N} \tag{7}$$

where K_L (L mg^{-1}) is the Langmuir constant, Q_{max} (mg g^{-1}) is the maximum adsorption capacity. C_m is the highest dye initial concentration, R_L indicates the affinity of adsorbent to adsorbate. In case of $R_L = 0$, the adsorption is irreversible; $0 < R_L < 1$, which is beneficial to adsorption; $R_L = 1$, which indicates linear adsorption; $R_L > 1$, which suggests unfavourable adsorption.n and K_F (mg g^{-1}) are the Freundlich constant. K_S (L mg^{-1}) is the Sips isotherm constant, N indicates the system heterogeneity when the value of N is 1. The above equation is reduced to the Langmuir adsorption isotherm. On the other hand, when K_S or C_e approaches zero, the isotherm equation is reduced to Freundlich isotherm.

The relevant results and parameters are shown in Fig. 10b–d and Table 2. From Fig. 10b–d and Table 2, the equilibrium data fit better with the Langmuir model than others because the correlation constants ($R^2 = 0.9924$, 0.9847, 0.9868, and 0.9982) are highest at four different temperatures. The calculated Q_{max} (409.1 mg g^{-1}, 415.5 mg g^{-1}, 451.5 mg g^{-1}, and 489.7 mg g^{-1}) approximates the experimental Q_{max} (374.4 mg g^{-1}, 417.5 mg g^{-1}, 463.4 mg g^{-1}, and 492.7 mg g^{-1}), implying the monolayer adsorption exhibits control over the adsorption process [4]. Moreover, the values of R_L are between 0 and 1, demonstrating that the adsorption on the LS/OMMT is a favorable process. Additionally, the calculated value of the Freundlich constant n is greater than 1, which further illustrates the favorable condition for the adsorption and implys the monolayer adsorption exerts a controlling effect on the adsorption process.

Adsorption Thermodynamic Analysis

Temperature is a critical factor in the adsorption process as it affects the diffusion rate of adsorbate molecules and the adsorption capacity [2]. Furthermore, the corresponding thermodynamic parameters include the entropic change of adsorption (ΔH^0), the Gibbs free energy (ΔG^0), and the enthalpy change of adsorption (ΔS^0), which can judge the absorption and heat release of the adsorption process, the spontaneity of the adsorption reaction and the degree of chaos in the adsorption process, respectively. As a result, experimental data collected at various temperatures were utilized to compute thermodynamic parameters such as ΔH^0 (kJ mol^{-1}), ΔG^0 (kJ mol^{-1}), and ΔS^0 (J mol^{-1} K^{-1}) by the following equation [62]:

$$Lnk_d = \frac{\Delta S^0}{R} - \frac{\Delta H^0}{RT} \tag{8}$$

$$\Delta G^0 = -RTLnk_d \tag{9}$$

$$k_d = \frac{Q_e}{C_e} \tag{10}$$

where K_d (L g^{-1}) is an equilibrium constant, R represents the gas constant 8.314 (J mol^{-1} K^{-1}) and T (K) is the absolute temperature. ΔH^0 and ΔS^0 were calculated from the slope and the intercept of the plot of $\ln K_d$ versus 1/T, respectively (see Fig. 11).

As demonstrated in Table 3, ΔG^0 are negative at all temperatures tested, showing that the adsorption is spontaneous [64]. Furthermore, ΔG^0 decreases as the temperature increases, indicating that higher temperatures are more favourable for adsorption. A positive ΔS^0 value confirmed

Table 2 The isothermal adsorption model parameters

Isotherm model	Parameters	Temperature (K)			
		283.15	293.15	303.15	313.15
Freundlich	1/n	0.3468	0.2649	0.1949	0.1764
	K_F (L mg^{-1})	62.23	108.2	179.8	208.8
	R^2	0.9584	0.9556	0.9374	0.9386
Langmuir	Q_{max} (mg g^{-1})	409.1	415.5	451.5	489.7
	K_L (L mg^{-1})	3.324×10^{-2}	6.846×10^{-2}	1.892×10^{-2}	2.074×10^{-2}
	R_L	6.266×10^{-2}	3.144×10^{-2}	1.161×10^{-2}	1.061×10^{-2}
	R^2	0.9924	0.9847	0.9868	0.9982
Sips	N	0.5346	0.6742	0.6820	0.3546
	K_S (L mg^{-1})	0.4143	0.1424	0.06641	0.4135
	Q_S (mg g^{-1})	537.3	563.9	593.8	659.1
	R^2	0.9874	0.9858	0.9873	0.9854

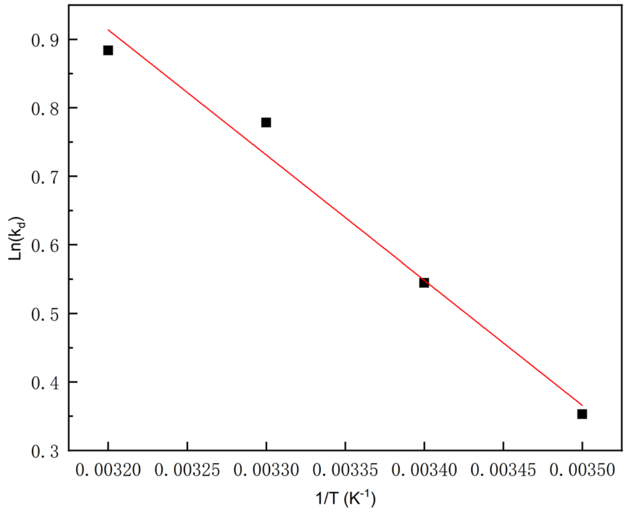

Fig. 11 The plot of $\ln K_d$ versus 1/T

Table 3 Thermodynamic parameter for MB adsorption on LS/OMMT

T (K)	ΔG° (kJ mol^{-1})	ΔH° (kJ mol^{-1})	ΔS° (J mol^{-1} K^{-1})
283	− 0.8300	15.18	56.24
293	− 1.326		
303	− 1.961		
313	− 2.229		

the enhanced unpredictability at the solid/liquid interface during adsorption. The positive value of ΔH^0 demonstrates the endothermic nature of the adsorption process, which is supported by the higher temperature adsorption capability. It is believed that LS/OMMT hydrogel is a polymer material with a three-dimensional network structure. This material shrinks at low temperature and expands at high temperature when it gets energy, that is to say, it can swell and form pores to boost dye adsorption [63]. In addition, high temperatures can increase the fluidity of dye molecules, enabling them to penetrate LS/OMMT gel layer [64]. In general, the ΔG° for physisorption ranges from − 20 to 0 kJ mol^{-1}, whereas chemisorption ranges from − 80 to − 400 kJ mol^{-1} [45]. Therefore, it can be determined that the adsorption of MB on LS/OMMT is a physical process. Furthermore, similar results have been found for MB adsorption on lignin cross-linked composite [65].

Effect of Contact Time and Adsorption Kinetics

The effect of contact time on the adsorption of MB onto the adsorbent LS/OMMT is shown in Fig. 12a. The influence of contact time and starting dye concentrations on Q_e was investigated by adding 100 mg of LS/OMMT to 200 mL MB solution (pH 7.0) at 293.15 K. For four different initial dye concentrations (100 mg L^{-1}, 200 mg L^{-1}, 300 mg L^{-1}, and 400 mg L^{-1}), the adsorption process was rapid during the first 40 min because of an abundance of adsorption sites on LS/OMMT. As the adsorption process progressed, the number of vacant adsorption sites on the outer surface reduced, slowing down the adsorption rate until equilibrium [61]. The adsorption equilibrium was established at about 80 min to 140 min, and the maximum Q_e was 180.4 mg g^{-1}, 314.2 mg g^{-1}, 375.1 mg g^{-1}, and 417.1 mg g^{-1} with initial MB concentrations of 100 mg L^{-1}, 200 mg L^{-1}, 300 mg L^{-1}, and 400 mg L^{-1}, respectively. Moreover, it was observed that there was a a faster adsorption equilibrium at lower C_0 and a slower adsorption equilibrium at higher C_0. This finding arises from the fact that there are many available binding sites in lower C_0 than in higher C_0 solutions [38].

Adsorption kinetics is essential because the adsorption rate and mechanism can be derived from kinetic studies. In this study, the adsorption was treated using the Pseudo-first order [4], Pseudo-second order [4], Intraparticle diffusion [66]. Their equations are expressed as follows:

$$Q_t = Q_e(1 - e^{-k_1 t}) \tag{11}$$

$$Q_t = \frac{k_2 Q_e^2 t}{1 + k_2 Q_e t} \tag{12}$$

$$Q_t = k_p t^{0.5} + C \tag{13}$$

where C is the Intraparticle diffusion constant. k_1 (min^{-1}), k_2 (g mg^{-1} $min^{-1/2}$), k_p (mg g^{-1}) are the Pseudo-first-order, Pseudo-second-order, and Intraparticle diffusion adsorption rate constant, respectively. The fitted data and parameter values are shown in Fig. 12b–d and Table 4, respectively. The correlation coefficient (R^2) for the Pseudo-second order kinetic model is higher than than that of the Pseudo-first order kinetic model, and the Q_e of the model is near the experimental data. Therefore, it can be concluded that the Pseudo-second-order adsorption model is more suitable for describing the adsorption kinetics of MB on LS/OMMT. The data in Fig. 12d show multi-linear plots, and all curves have three parts: (i) the film diffusion stage 67] (ii) the intraparticle diffusion [68] and (iii) the equilibrium adsorption process. The result indicate that intraparticle diffusion is involved in the adsorption process [17]. Furthermore, the straight lines do not pass through the origin ($C \neq 0$), indicating that intraparticle diffusion is not the only rate-limiting step, and the film diffusion can simultaneously be interpreted in the adsorption kinetics [20, 21].

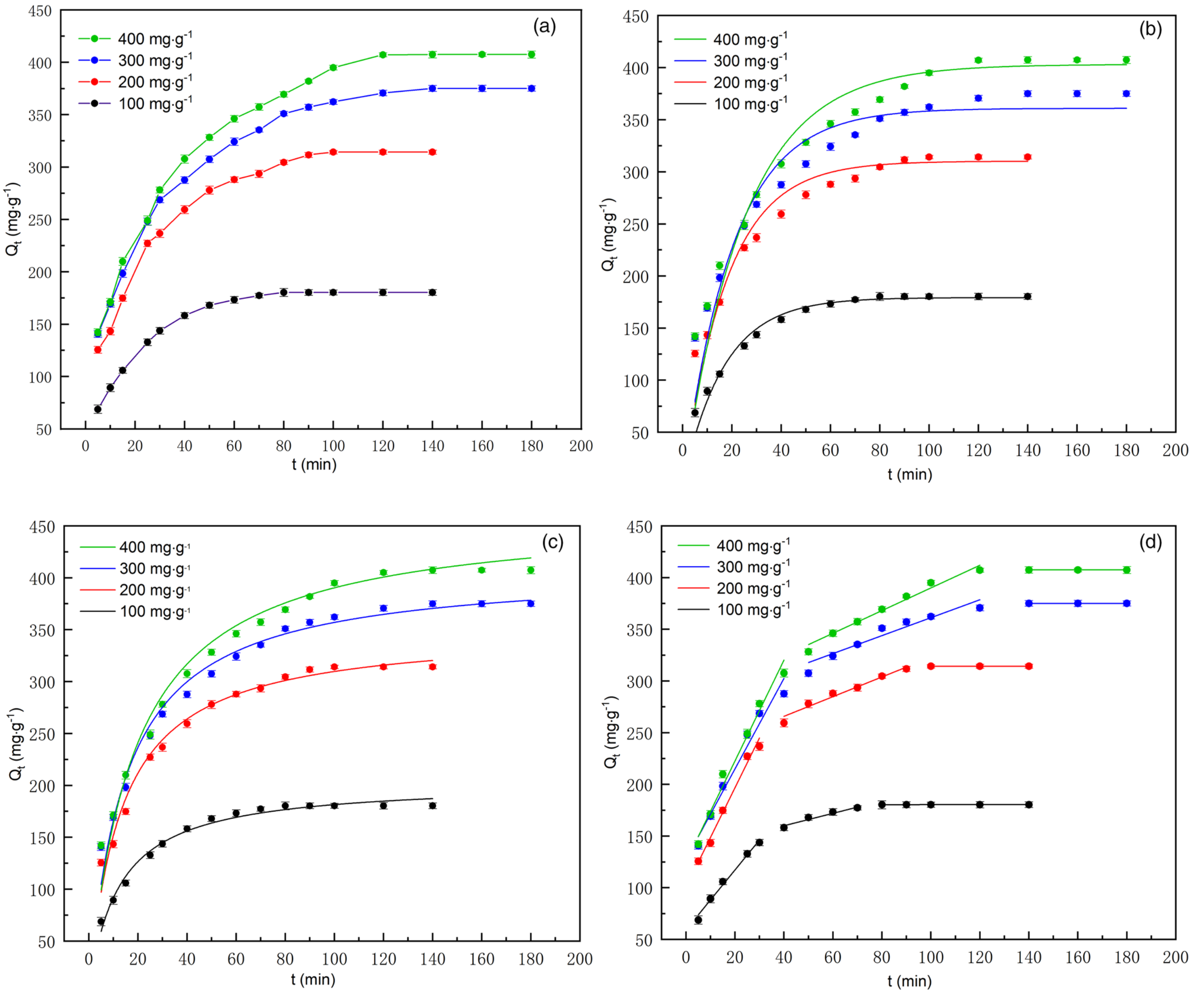

Fig. 12 The effect of contact time on adsorption of MB by LS/OMMT (**a**) (pH 7.0; absorbent dosage, 0.5 g L^{-1}; temperature, 293.15 K), adsorption kinetics: Pseudo-first order (**b**), Pseudo-second order (**c**), Intraparticle diffusion (**d**)

Table 4 Kinetic parameters for the adsorption

Kinetic models	Parameters	Concentration (mg L^{-1})			
		100	200	300	400
Pseudo-fifirst-order	Q_e (mg g^{-1})	203.6	356.2	409.2	453.7
	k_1 (min^{-1})	6.073×10^{-2}	5.612×10^{-2}	4.945×10^{-2}	4.013×10^{-2}
	R^2	0.9787	0.9493	0.9336	0.9372
Pseudo-second-order	Q_e (mg g^{-1})	179.3	310.2	360.9	409.6
	k_2 (g mg^{-1} min^{-1})	4.467×10^{-4}	2.278×10^{-4}	1.735×10^{-4}	1.241×10^{-4}
	R^2	0.9897	0.9866	0.9843	0.9821
Intraparticle diffusion	k_{p1} [mg (g min$^{0.5}$)$^{-1}$]	2.898	4.805	5.108	5.334
	C_1	59.53	100.7	117.8	119.3
	$(R_1)^2$	0.9887	0.9565	0.9983	0.9924
	k_{p2} [mg (g min$^{0.5}$)$^{-1}$]	0.6013	0.9525	1.196	1.363
	C_2	136.0	227.8	278.2	260.0
	$(R_2)^2$	0.9814	0.9702	0.9752	0.9923

Adsorbent Comparison

In order to evaluate the adsorption performance of LS/OMMT toward MB, its maximum Q_e was compared with some other reported ones in the literature, as summarized in Table 5. It is clear that LS/OMMT is a promising candidate for the removal of MB removal from wastewater, in view of the maximum Q_e and pH values.

Reusability Study

One of the essential properties of adsorbents used to remove dyes from wastewater is their ability to maintain their adsorption capacity over multiple adsorption–desorption cycles [25]. Figure 13 shows that the RR can retain more than 84% after five cycles. This desorption behavior can be detected because H^+ ions rapidly replace the cationic dye molecules in acidic conditions, showing that the MB is attached to the hydrogel by electrostatic contact. Since the H^+ ions linked to the binding point of the hydrogel are replaced by OH^- present in the NaOH solution, the desorbed materials are highly effective in reabsorbing the MB after being regenerated. As can be seen from the above results, LS/OMMT exhibits good reusability.

Adsorption Mechanism

FT-IR and XPS were carried out to explore the mechanism of MB adsorption on LS/OMMT. FT-IR spectra of LS/OMMT before and after adsorbing MB (MB-LS/OMMT) were recorded to understand the adsorption mechanism. The results are shown in Fig. 14a. After MB adsorption, three additional peaks of MB are detected around 1593 cm^{-1}, 1332 cm^{-1}, and 1355 cm^{-1}, which are connected to the bending vibrations of $–CH_3$, the stretching vibrations of $(CH_3)_2N–$, and the stretching vibration of C=N of the MB heterocycle, respectively [69]. Additionally, the peaks at 1729 cm^{-1} (–COOH) and 1114 cm^{-1} ($–SO_3$) shift to 1716 cm^{-1} and 1119 cm^{-1} after adsorption, implying the involvement of carboxyl and sulfonic acid groups in the adsorption process. At 3410 cm^{-1}, peaks were overlapping –NH/–OH stretching vibration grew more substantial and broader. It can be explained by hydrogen-bonding interactions between the surface groups of LS/OMMT and MB [4].

To gain further insight into the interactions between MB and LS/OMMT, XPS studies of LS/OMMT and MB-LS/OMMT were undertaken. As shown in Fig. 14b, photoelectron peaks exist at 73.50 (Al 2p) and 120.58 (Si 2p) eV, indicating that the OMMT was successfully embedded into the hydrogel matrix.

The high-resolution XPS spectra of N1s spectra of LS/OMMT can be fit by three peaks with binding energies of 398.67 eV (N–H), 399.37 eV (H–N–H), and 399.97 eV (O=C–N), respectively. According to the literature [70], the

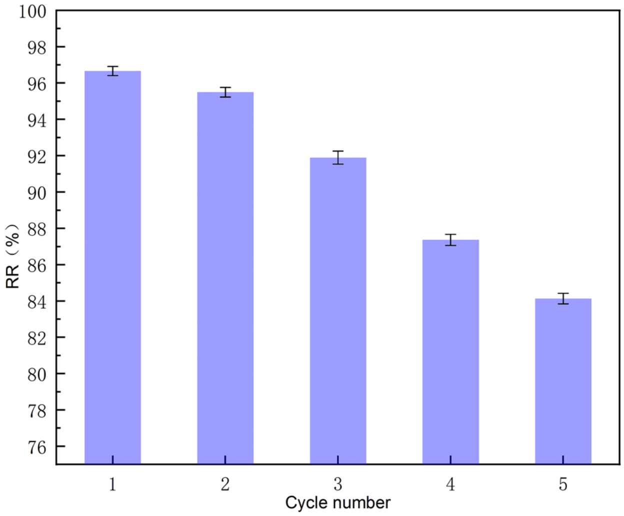

Fig. 13 Adsorption desorption cycles for LS/OMMT(adsorption conditions: initial MB concentration, 50 mg L^{-1}; pH 7.0; absorbent dosage, 0.5 g L^{-1}; temperature, 293.15 K; contact time, 140 min; desorption conditions: temperature, 293.15 K; contact time, 24 h)

Table 5 Comparison of the MB maximum adsorption capacities on LS/OMMT

Adsorbents	Conditionds(dye concentration (mg L^{-1}), temperature (°C), pH, time(minutes))	Q_{max} (mg g^{-1})	References
Carbon/montmorillonite	140, 25, 8, 60	138	[3]
Chitosan-MMT/PEI	100, 25, 7, 120	111	[4]
Cellulose/MMT	100, 25, 7, 3600	277	[73]
Graphene/magnetite/MMT	100, 25, 11, 20	255	[74]
Fe_3O_4/activated MMT	120, 25, 7, 25	120	[48]
Activated lignin-chitosan	82, 20, 7, 2400	36.3	[75]
Montmorillonite clay	1000, 60, 11, 2400	300	[76]
CMC-PAA-GO	70, 30, 8, 3600	63	[77]
PVA/PCMC/bentonite	200, 40, 8, 120	157.5	[78]
LS/OMMT	450, 40, 7, 140	492.7	This study

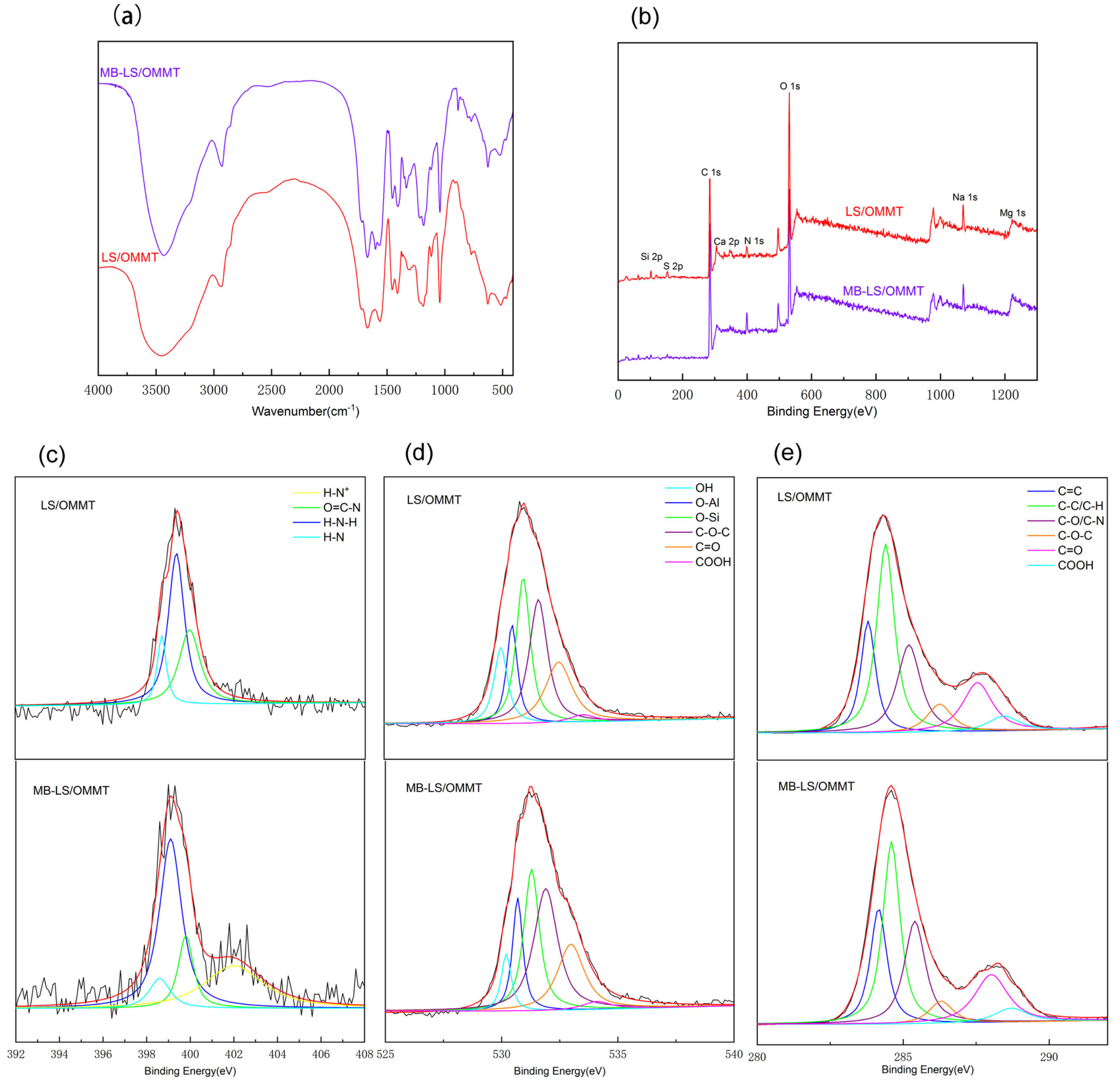

Fig. 14 FT-IR of LS/OMMT before and after adsorption (MB-LS/OMMT) (**a**), wide scan XPS spectrum of LS/OMMT before and after adsorption MB (**b**), high-resolution XPS spectra of N1s, O1s and C1s (**c**, **d**, **e**) for LS/OMMT before and after MB adsorption

positive charge in MB molecules is uniformly distributed as a result of the delocalized π bond and the nitrogen atoms in the MB molecule are in the same chemical state. Therefore, the high-resolution N1s scan spectrum of the MB molecule is symmetrical without splitting, and the binding energy (BE) peak is visible at 399.1 eV. Following MB adsorption, a new peak with binding energies of 402.03 eV (HN^+) appears in Fig. 14c, which is more robust than the BE of N1s of NH_4Cl (401.50 eV). It can be inferred that the nitrogen atom in the MB molecule was involved in MB adsorption via hydrogen bonding and electrostatic attraction. When MB is adsorbed on the surface of LS/OMMT, the positive charge of MB is concentrated on this nitrogen atom, and this positive charge must be on the nitrogen atom of dimethylamino groups to retain the most stable MB molecule [71].

The high-resolution XPS spectra of C1s and O1s for LS/OMMT are shown in Fig. 14d and e. The fitted O1s XPS spectra are shown in Fig. 14d with peaks at 529.98 eV, 530.52 eV, 531.12 eV, 531.55 eV, 532.40 eV, and 533.56 eV, respectively, corresponding to O–H, O–Al, O–Si, C–O–C,

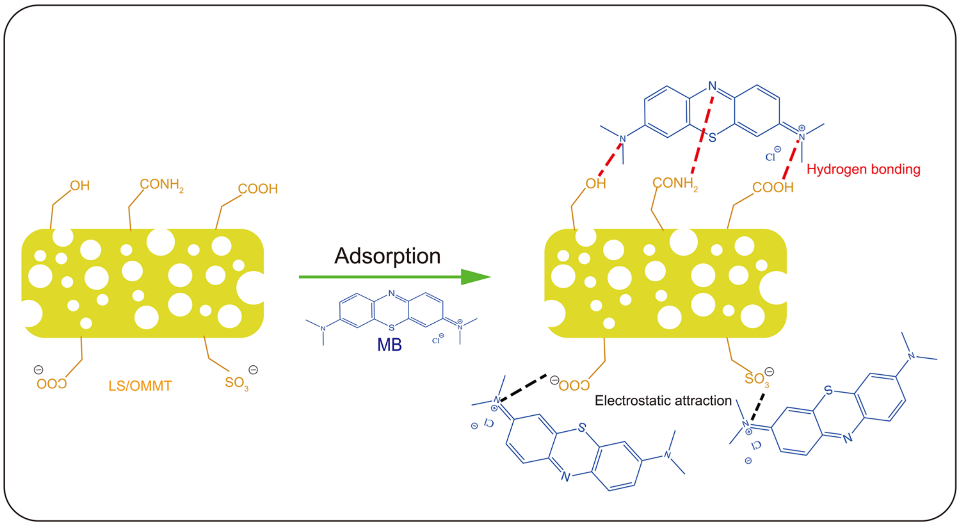

Fig. 15 Schematic illustration of the interaction mechanism between MB and LS/OMMT

O=C, and COOH [19]. The peaks of C1s are at 283.63 eV, 284.14 eV, 285.20 eV, 286.21 eV, 287.64 eV, and 288.41 eV, corresponding to C=C, C–C/C-H, C-O/C-N, C–O–C, C=O, and COOH. After MB adsorption, the peaks of O–H, O-C-O, and COOH shift to 530.21 eV, 531.87 eV, and 533.81 eV in Fig. 14d and shift to 285.39 eV, 286.37 eV, and 288.74 eV [25, 72] in Fig. 14e, implying that the functional groups mentioned above are involved in the adsorption process. In conclusion, the proposed uptake mechanism is shown in Fig. 15.

Conclusions

A new lignin-based hybrid hydrogel (LS/OMMT) was prepared by free radical polymerization and served as an adsorbent to remove MB from aqueous solutions. Under the optimized adsorption conditions, the adsorbent exhibited an adsorption capacity of 492.7 mg g^{-1} at 313.15 K and pH 7.0. Adsorption of MB from the LS/OMMT could be easily achieved by electrostatic attraction and hydrogen bonding. In addition, desorption studies predicted that the hydrogel could preserve relatively high reusability. This study demonstrates that LS/OMMT has emerged as a promising adsorbent for the removal of dyes from aqueous solutions.

Author Contributions LS: Material preparation, data collection, analysis, and writing-original draft; WL: Material preparation and data collection; XZ: Review of previous versions of the manuscript and funding acquisition; JH: Funding acquisition.

Funding This work was funded by the Anhui Outstanding Youth Funding of Anhui Province (1908085J10) and the Natural Science Foundation of China (21671004).

Declarations

Conflict of interest The authors declare that there are no conflict of interest.

References

1. Hasan Z, Jhung SH (2015) Removal of hazardous organics from water using metal-organic frameworks (MOFs): plausible mechanisms for selective adsorptions. J Hazard Mater 283(11):329–339
2. Liu F, Zou HL, Hu JW, Liu HB, Peng JB, Chen YW, Liu FHL, Huo YP (2016) Fast removal of methylene blue from aqueous solution using porous soy protein isolate based composite beads. Chem Eng J 287(1):410–418
3. Tong DS, Tong CW, Adebajo MO, Jin GC, Yu WH, Ji SF, Zhou CH (2018) Adsorption of methylene blue from aqueous solution onto porous cellulose derived carbon/montmorillonite nanocomposites. Appl Clay Sci 161(1):256–264
4. Minisy IM, Salahuddin NA, Ayad MM (2021) Adsorption of methylene blue onto chitosan- montmorillonite /polyaniline nanocomposite. Appl Clay Sci 203(15):105993
5. Guo R, Jiao T, Li R, Chen Y, Guo W, Zhang L, Zhou J, Zhang Q, Peng Q (2017) Sandwiched Fe$_3$O$_4$/carboxylate graphene oxide nanostructures constructed by layer-by-layer assembly for highly efficient and magnetically recyclable dye removal. ACS Sustain Chem Eng 6(1):1279–1288
6. Naik AP, Mittal H, Wadi VS, Sane L, Raj A, Alhassan SM, Alili AA, Bhosale SV, Morajkar PP (2020) Super porous TiO$_2$ photocatalyst: tailoring the agglomerate porosity into robust structural mesoporosity with enhanced surface area for efficient remediation of azo dye polluted waste water. J Environ Manag 258(15):110029
7. Liu Y, Zhao Y, Cheng W, Zhang T (2020) Targeted reclaiming cationic dyes from dyeing wastewater with a dithiocarbamate-functionalized material through selective adsorption and efficient desorption. J Colloid Interf Sci 579(1):766–777
8. Morshed MN, Pervez MN, Behary N, Bouazizi N, Guan J, Nierstrasz VA (2020) Statistical modeling and optimization of heterogeneous fenton-like removal of organic pollutant using fibrous catalysts: a full factorial design.Sci Rep 10:16133.
9. Oulad F, Zinadini S, Zinatizadeh AA, Derakhshan AA (2020) Fabrication and characterization of a novel tannic acid coated

boehmite/PES high performance antifouling NF membrane and application for licorice dye removal. Chem Eng J 397(1):125105

10. Bhatnagar A, Sillanpää M, Witek-Krowiak A (2015) Agricultural waste peels as versatile biomass for water purification—a review. Chem Eng J 270(15):244–271
11. Gao W, Zhao S, Wu H, Deligeer W, Aauha S (2016) Direct acid activation of kaolinite and its effects on the adsorption of methylene blue. Appl Clay Sci 126:98–106
12. Nakagawa K, Namba A, Mukai SR, Tamon H, Ariyadejwanich P, Tanthapanichakoon W (2004) Adsorption of phenol and reactive dye from aqueous solution on activated carbons derived from solid wastes. Water Res 38(7):1791–1798
13. Woolard C, Strong J, Erasmus C (2002) Evaluation of the use of modified coal ash as a potential sorbent for organic waste streams. Appl Geol Chem 17(8):1159–1164
14. Zhang C, Liu Y, Sun L, Shi H, Shi C, Liang Z, Li J (2018) A zwitterionic ligand-based cationic metal-organic framework for rapidly selective dye capture and highly efficient $Cr_2O_7^{2-}$ removal. Chemistry 24(11):2718–2724
15. Madan S, Shaw R, Tiwari S, Tiwari SK (2019) Adsorption dynamics of congo red dye removal using ZnO function-alized high silica zeolitic particles. Appl Surf Sci 487(1):907–917
16. Cyras VP, Manfredi LB, Ton-That MT, Vazquez A (2008) Physical and mechanical properties of thermoplastic starch/montmorillonite nanocomposite films. Carbohydr Polym 73(1):55–63
17. Lu J, Jin R, Liu C, Wang Y, Yang X (2016) Magnetic carboxylated cellulose nanocrystals as adsorbent for the removal of Pb(II) from aqueous solution. Int J Biol Macromol 93:547–556
18. Ibrahim AG, Sayed AZ, El-Wahab HA, Sayah MM (2020) Synthesis of a hydrogel by grafting of acrylamide-co-sodium methacrylate onto chitosan for effective adsorption of fuchsin basic dye. Int J Biol Macromol 159(15):422–432
19. Ma YI, Lv L, Guo YR, Fu J, Shao Q, Wu TT, Guo SJ, Sun K, Guo XK, Wujcik EK, Guo ZH (2017) Porous lignin based poly (acrylic acid)/organo-montmorillonite nanocomposites: Swelling behaviors and rapid removal of Pb (II) ions. Polymer 128(16):12–23
20. Ahmad MA, Eusoff MA, Adegoke KA, Bello OS (2021) Sequestration of methylene blue dye from aqueous solution using microwave assisted dragon fruit peel as adsorbent. Environ Echnol Innov 24:101917
21. Klapiszewski L, Bartczak P, Wysokowski M, Jankowska M, Kabat K, Jesionowski T (2015) Silica conjugated with kraft lignin and its use as a novel ‘green’ sorbent for hazardous metal ions removal. Chem Eng J 260(15):684–693
22. Ciesielczyk F, Bartczak P, Klapiszewski L, Jesionowski T (2017) Treatment of model and galvanic waste solutions of copper(II) ions using a lignin/inorganic oxide hybrid as an effective sorbent. J Hazard Mater 328:150–159
23. Klapiszewski L, Siwińska-Stefańska K, Kołodyńska D (2017) Preparation and characterization of novel TiO_2/lignin and TiO_2–SiO_2/lignin hybrids and their use as functional biosorbents for Pb(II). Chem Eng J 314(15):169–181
24. Yu CH, Wang F, Zhang CH, Fu SY, Lucia LA (2016) The synthesis and absorption dynamics of a lignin-based hydrogel for remediation of cationic dye-contaminated effluent. React Funct Polym 106:137–142
25. Shi XX, Qiao YY, An XX, Tian YY, Zhou HF (2020) High-capacity adsorption of Cr(VI) by lignin-based composite:Characterization, performance and mechanism. Int J Biol Macromol 159(15):839–849
26. Unnikrishnan L, Mohanty S, Nayak SK, Ali A (2011) Preparation and characterization of poly(methyl methacrylate)-clay nanocomposites via melt intercalation: effect of organoclay on thermal, mechanical and flammability properties. Mater Sci Eng A 528(12):3943–3951
27. Adeyemo AA, Adeoye IO, Bello OS (2017) Adsorption of dyes using different types of clay: a review. Appl Wate Sci 7:543–568
28. Zheng X, Jiang DD, Wilkie CA (2006) Polystyrene nanocomposites based on an oligomerically -modified clay containing maleic anhydride. Polym Degrad Stab 91(1):108–113
29. Taleb MFA, Hegazy DE, Ismail SA (2012) Radiation synthesis, characterization and dye adsorption of alginate-organophilic montmorillonite nanocomposite. Carbohydr Polym 87:2263–2269
30. Wu RL, Tian LY, Wang W (2015) Synthesis of a nanocomposite of organo-montmorillonite/cellulose -g-poly(methyl methacrylate) by atom-transfer radical polymerization and its application in removal of 2,4-dichlorophenol. Cellulose 2:3633–3643
31. Wang Y, Xiong Y, Wang JY, Zhang XD (2017) Ultrasonic-assisted fabrication of montmorillonite -lignin hybrid hydrogel: Highly efficient swelling behaviors and super-sorbent for dye removal from wastewater. Colloid Surface A 520:903–913
32. Sun XF, Hao YW, Cao YY, Zeng QH (2019) Superadsorbent hydrogel based on lignin and montmorillonite for Cu(II) ions removal from aqueous solution. Int J Biol Macromol 127:511–519
33. Unuabonah EI, Adie GU, Onah LO, Adeyemi OG (2009) Multistage optimization of the adsorption of methylene blue dye onto defatted Carica papaya seeds. Chem Eng J 155:567–579
34. Pan H, Sun G, Zhao T (2013) Synthesis and characterization of aminated lignin. Int J Biol Macromol 59:221–226
35. Zenat A, Amira AEG, Samia H, Beshay U (2001) Biochemical modification of lignin by fungi species. IPPTA 13(2):19–32
36. Klapiszewski A, Wysokowski M, Majchrzak I, Szatkowski T, Nowacka M, StefaNska KS, Rzepka KS, Bartczak PB, Ehrlich H, Jesionowski T (2013) Preparation and characterization of multifunctional chitin/lignin materials. J Nanomater 2013:1–13
37. Yao Q, Xie J, Liu J, Kang HM, Liu Y (2014) Adsorption of lead ions using a modified lignin hydrogel. J Polym Res 21(6):6–16
38. Tang YF, Zeng YD, Hu T, Zhou Q, Peng YZ (2016) Preparation of lignin sulfonate-based mesoporous materials for adsorbing malachite green from aqueous solution. J Envron Eng 4:2900–2910
39. Rémond C, Aubry N, Crônier D (2010) Combination of ammonia and xylanase pretreatments: impact on enzymatic xylan and cellulose recover from wheatstraw. Bioresour Technol 101(17):6712–6717
40. Du PY, Ke ZJ, Liu JX, Wang T, Chen S, Mei M, Li JP, Zhu SJ (2022) A highly efficient biomass-based adsorbent fabricated by graft copolymerization: Kinetics, isotherms, mechanism and coadsorption investigations for cationic dye and heavy metal. J Colloid Interf Sci 616(15):12–22
41. Tahari N, Hoyos-Martinez PLD, Abderrabba M, Ayadi S, Labidi J (2020) Lignin-montmorillonite hydrogels as toluene adsorbent. Colloids Surf A 602(5):125108
42. Mashael A, Amal AA, Waffa M (2013) Polystyrene/montmorillonite nanocomposites: study of the morphology and effects of sonication time on thermal stability. J Nanomater 2013:650725
43. Chipera SJ, Bish DL (2001) Baseline studies of the clay minerals society source clays:powder X-ray diffraction analyses. Clay Clay Miner 49(5):398–409
44. Essawya HA, Ghazy MBM, El-Hai FA, Mohamedb MF (2016) Superabsorbent hydrogels via graft polymerization of acrylic acid from chitosan-cellulose hybrid and their potential in controlled release of soil nutrients. Int J Biol Macromol 89:144–151
45. Karaca S, Nal EA, Al Z, Khataee A (2021) Preparation of chitosan modified montmorillonite biocomposite for sonocatalysis of dyes: Parameters and degradation mechanism. Mater Chem Phys 260(15):124125
46. Jawad AH, Abdulhameed AS (2020) Mesoporous Iraqi red kaolin clay as an efficient adsorbent for methylene blue dye: adsorption kinetic, isotherm and mechanism study. Surf Interfaces 18:100422

47. Chang JL, Ma JC, Ma QL, Zhang DD, Qiao NN, Hu MX, Ma HZ (2018) Adsorption of methylene blue onto Fe_3O_4/activated montmorillonite nanocomposite. Appl Clay Sci 161:256–264
48. Liu D, Yuan WW, Deng LL, Yu WB, Sun HJ, Yuan P (2014) Preparation of porous diatomite-templated carbons with large adsorption capacity and mesoporous zeolite KH as a byproduct. J Colloid Interface Sci 424:22–26
49. Sing KS (1984) Reporting physisorption data for gas/solid systems with special reference to the determination of surface area and porosity, (Recommendations 1984). Pure Appl Chem 57:603–619
50. Brunauer S, Emmett PH, Teller E (1938) Adsorption of gases in multimolecular layers. J Am Chem Soc 60:309–319
51. Karmanov AP, Kanarsky AV, Kanarskaya ZA, Kocheva LS, Semenov EI, Bogdanovich NI, Belyy VA (2020) In vitro adsorption-desorption of aflatoxin B1 on Pepper's lignins isolated from grassy plants. International Int J Biol Macromol 144:111–117
52. Pi Z, Hou K, Yao F, He L, Chen S, Tao Z, Zhou P, Wang D, Li X, Yang Q (2022) In-situ regeneration of tetracycline-saturated hierarchical porous carbon by peroxydisulfate oxidation process: performance, mechanism and application. Chem Eng J 427(1):131749
53. Yan B, Chen ZH, Cai L, Chen ZM, Fu JW, Xu Q (2015) Fabrication of polyaniline hydrogel: synthesis characterization and adsorption of methylene blue. Appl Surf Sci 356(30):39–47
54. Shen YF, Zhang NY (2019) Facile synthesis of porous carbons from silica-rich rice husk char for volatile organic compounds (VOCs) sorption. Bioresour Technol 282:294–300
55. Yan TT, Chen H, Wang X, Jiang F (2013) Adsorption of perfluorooctane sulfonate (PFOS) on mesoporous carbon nitride. RSC Adv 3(44):22480–22489
56. Wang QH, Zhu LX, Sun LQ, Liu YC, Jiao LF (2015) Facile synthesis of hierarchical porous ZnCo2O4 microspheres for high-performance supercapacitors. J Mater Chem A 3:982–985
57. Monvisade P, Siriphannon P (2009) Chitosan intercalated montmorillonite: preparation, characterization and cationic dye adsorption. Appl Clay Sci 42:427–431
58. Sharma G, Naushad M, Kumar A, Rana S, Sharma S, Bhatnagar A, Stadler FJ, Ghfar AA, Khan MR (2017) Efficient removal of coomassie brilliant blue R-250 dye using starch/poly(alginic acid-cl-acrylamide) nanohydrogel. Process Saf Environ 109:301–310
59. Dadhaniya PV, Patel MP, Patel RG (2007) Removal of anionic dyes from aqueous solution using poly [N-vinyl pyrrolidone/2-(methacryloyloxyethyl) trimethyl ammonium chloride super swelling hydrogels. Polym Bull 58:359–369
60. Ghorai S, Sarkar A, Raoufi M, Panda AB, Schonherr H, Pal S (2014) Enhanced removal of methylene blue and methyl violet dyes from aqueous solution using a nanocomposite of hydrolyzed polyacrylamide grafted xanthan gum and incorporated nanosilica. ACS Appl Mater Inter 6(7):4766–4777
61. Ghouti MA, Absi RS (2020) Mechanistic understanding of the adsorption and thermodynamic aspects of cationic methylene blue dye onto cellulosic olive stones biomass from wastewater. Sci Rep 10:15928
62. Tang Z, Hu XS, Ding HY, Li ZJ, Liang R, Sun GX (2021) Villi-like poly(acrylic acid) based hydrogel adsorbent with fast and highly efficient methylene blue removing ability. J Colloid Interfaces Sci 594(15):54–63
63. Sabe SS, Saber SS, Gazi M (2013) Cellulose-graft-polyacrylamide /hydroxyapatite composite hydrogel with possible application in removal of Cu(II) ions. React Funct Polym 73(11):1523–1530
64. Moussavi G, Alahabadi A, Yaghmaeian K, Eskandari M (2013) Preparation, characterizationa and adsorption potential of the NH_4Cl-induced activated carbon for the removal of amoxicillin antibiotic from water. Chem Eng J 217(1):119–128
65. Aishafey ESI, Ailawati H, Aisumri AS (2012) Ciproflfloxacin adsorption from aqueous solution onto chemically prepared carbon from date palm leaflflets. J Environ Sci 24(9):1579–1586
66. Shovsky A, Bijelic G, Varga I, Makuska R, Claesson PM (2011) Adsorption characteristics of stoichiometric and nonstoichiometric molecular polyelectrolyte complexes on silicon oxynitride surfaces. Langmuir 27:1044–1050
67. Albadarin AB, Collins MN, Naushad M, Shirazian S, Walker G, Mangwandi C (2017) Activated lignin-chitosan extruded blends for efficient adsorption of methylene blue. Chem Eng J 307(1):264–272
68. Ameida CAP, Debacher NA, Downs AJ, Cottet L, Mello CAD (2009) Removal of methylene blue from colored effluents by adsorption on montmorillonite clay. J Colloid Interf Sci 332:46–53
69. Liu XJ, Li MF, Ma JF, Bian J, Peng F (2022) Chitosan crosslinked composite based on corncob lignin biochar to adsorb methylene blue: Kinetics, isotherm, and thermodynamics.Colloid Surface A 642(5):128621.
70. Reichenberg D (1953) Properties of ion exchange resins in relation to their structure.III. Kinetics of exchange, J Am Chem Soc 75:589–598
71. Wang QY, Wang YX, Chen LY (2019) A green composite hydrogel based on cellulose and clay as efficient absorbent of colored organic effluent. Carbohydr Polym 210(15):314–321
72. Zhang B, Zhang TL, Zhang ZD, Xie MY (2019) Hydrothermal synthesis of a graphene /magnetite/montmorillonite nanocomposite and its ultrasonically assisted methylene blue adsorption. J Mater Sci 54:11037–11055
73. Dai HJ, Huang Y, Huang HH (2018) Eco-friendly polyvinyl alcohol/carboxymethyl cellulose hydrogelsreinforced with graphene oxide and bentonite for enhanced adsorption of methylene blue. Carbohydr Polym 185:1–11
74. Wang W, Zhao YL, Bai HY, Zhang TT, Galvan VI, Song SX (2018) Methylene blue removal from water using the hydrogel beads of poly(vinyl alcohol)-sodium alginate-chitosan-montmorillonite. Carbohydr Polym 198(15):518–528
75. Ozcan AS, Ozcan A (2004) Adsorption of acid dyes from aqueous solutions onto acid activated bentonite. J Colloid Interface Sci 276(1):39–46
76. Zhao LY, Wang XK, Guo YG (2003) Adsorption of methylene blue on the muscovite. Acta Phys Chim Sin 19(10):896–901
77. Kang SC, Zhao YL, Wang W, Zhang TT, Chen TX, Yi H, Rao F, Song SX (2018) Removal of methylene blue from water with montmorillonite nanosheets/chitosan hydrogels as adsorbent. Appl Surf Sci 448(1):203–211
78. Thakur B, Sharma G, Kumar A, Sharma S, Naushad M, Iqbal J, Stadler FJ (2020) Designing of bentonite based nanocomposite hydrogel for the adsorptive removal and controlled release of ampicillin. J Mol Liq 319(1):114166